

1 **Better constraining the geometry of faults in the
2 Charlevoix Seismic Zone using a modified Optimal
3 Anisotropic Dynamic Clustering (OADC) algorithm**

4 **Oluwaseun Idowu Fadugba¹, Charles Langston¹, Christine A. Powell¹, and
5 Eunseo Choi¹**

6 ¹Center for Earthquake Research and Information, The University of Memphis, Memphis, TN 38152

7 **Key Points:**

- 8 • The first fault dips at an angle of 60° while the other two main rift faults dip at
9 44° and 43° , respectively. These fault geometries match the work by Powell and
10 Lamontagne (2017).
- 11 • The rift faults show a more complicated geometry than the simple three-faults model
12 in previous works, especially within the crater region.
- 13 • The rift fault to the northwest of the crater changes in strike and dip. The fault
14 dips about 60°SE outside the crater, but has shallower dips of about 33.4° and
15 34.8° within the crater.

Corresponding author: Oluwaseun Idowu Fadugba, ifadugba@memphis.edu

16 **Abstract**

17 The Charlevoix Seismic Zone (CSZ) occurs along the early Paleozoic St. Lawrence rift
 18 zone in southeastern Quebec at the location of a major Devonian impact crater. The crater
 19 superimposed three major basement faults trending N35°E. Previous work suggests two
 20 sets of geometries for the rift faults. One set has a uniform dip of 70°SE for all three faults
 21 while the other has 65°, 40°, and 40°SE, from north to south, respectively. Visual es-
 22 timation of fault planes from over 1300 relocated hypocenters in the CSZ suggests more
 23 complex fault geometry. We apply the Optimal Anisotropic Dynamic Clustering (OADC)
 24 algorithm to model realistic fault planes that best fit the hypocenter data. OADC method
 25 is a generalization of the k-means method using randomly-seeded planes to partition hypocen-
 26 ters into clusters. OADC uses the eigenvalue-eigenvector analysis of the covariance of
 27 hypocenter locations by minimizing the smallest eigenvalues of each cluster. The eigen-
 28 values and eigenvectors of each cluster are related to the fault dimension and orienta-
 29 tion, respectively. We will extend the OADC method by incorporating high-quality source
 30 mechanisms of the earthquakes to specify seed planes rather than using randomly-seeded
 31 planes. We will also present a new method of clustering earthquakes on planes by pro-
 32 jecting the hypocenters on differently oriented planes.

33 **1 Introduction**

34 The Charlevoix Seismic Zone (CSZ) occurs along the early Paleozoic St. Lawrence
 35 rift zone in southeastern Quebec at the location of a major Devonian impact crater. The
 36 crater superimposed three major basement faults trending N35°E. The CSZ poses higher
 37 risks due to its seismicity compared to the other seismic zones in the area and its prox-
 38 imity to densely populated cities (e.g. Quebec City, Ottawa and Montreal). Other seis-
 39 mic zones in Eastern Canada are Lower St. Lawrence (LSL), Ottawa-Bonnechere graben
 40 (OBQ), Western Quebec seismic zone (WQ) and the Saguenay graben (SG) (Fig. ??,
 41 ??). The CSZ poses higher risks due to its history of generating large earthquakes. CSZ
 42 is the most active seismic zone in the southwestern Canada (?) and has housed large earth-
 43 quakes, up to M6.5 in 1925 (?) and M7.5 in 1663 (?).

44 The tectonic history of the CSZ can be broadly divided into four parts. They are:
 45 the Grenville orogeny (1100-990 Ma) reflected in amphibolite to granulite metamorphic
 46 basement rocks, the breakup of the basement terrains which formed the Iapetus Ocean,
 47 Appalachian orogeny formed by the closing of the Iapetus ocean, and the impact crater

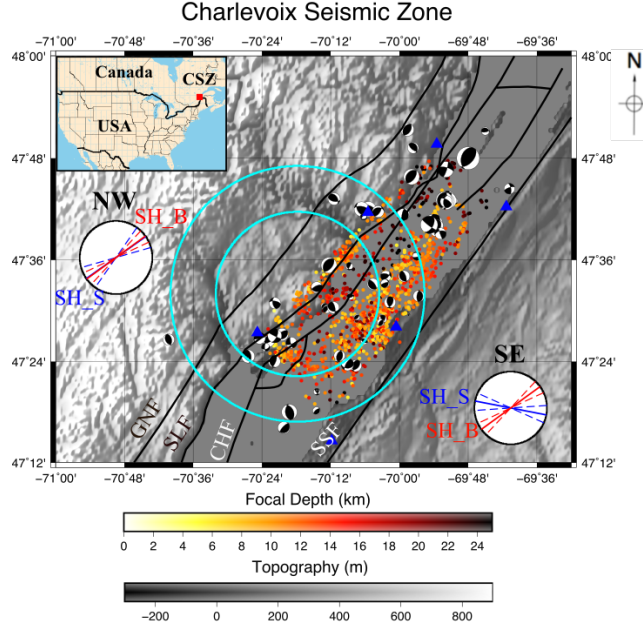


Figure 1. Topography and seismicity of the Charlevoix Seismic Zone (CSZ) as well as the locations of the impact crater (outer cyan circle) and the more damaged inner crater (inner cyan circle). Small circles are the relocated epicenters (?) and their colors represent the focal depths. The focal mechanisms are for the earthquakes used by ? for the stress inversion. Large circles labeled as NW and SE show orientations of SH_{max} from the stress inversion of focal mechanism (SH_S) and from borehole breakout measurements (SH_B) for the earthquake clusters northwest and southeast of the crater center. Solid black lines mark the rift faults known in the region: GNF, Gouffre Northwest Fault; SLF, Saint-Laurent fault; CHF, Charlevoix Fault; and SSF, South Shore Fault (??). The inset shows the location of the CSZ in eastern Canada. Earthquake epicenters from the National Resources Canada catalog for the years 1988-2011.

in the Devonian (????). The basement rocks and Appalachian nappes outcrop in the NW and SE part of the CSZ, respectively, and are separated by Logan's line (Fig. 2). Logan's line runs through the center of the crater and along the "north" shore of the St. Lawrence River (Rondot 1994). The three major rift faults in the CSZ are the Gouffre Northwest Fault, Saint-Laurent fault, Charlevoix Fault (Powell and Lamontagne, 2017; Fadugba et al., 2019).

Powell and Lamontagne (2017) determined 3D V_p and V_s velocity model of the CSZ and relocated the earthquake using the 3D velocity model. Visual estimation of the epicenters in the CSZ shows two major earthquake clusters: the northwestern (NW) and

southeastern (SE) clusters. The NW clusters have earthquakes on the Gouffre Northwest fault while the SE clusters comprise of the earthquakes on the Saint-Laurent and Charlevoix faults. Powell and Lamontagne (2017) also observed circular arcs of seismicity that follow the edge of the impact structure found in 3D tomographic inversions. The presence of damaged crustal crust from the impact crater makes the CSZ an anomalous seismic zone. The presence of the impact crater should decreased the seismicity of the CSZ due to the damaged crustal rocks (Solomon et al.).

Previous works observed a unique distribution of earthquakes in the CSZ (e.g. Baird et al.) and a stress rotation in the CSZ relative to the regional first-order maximum horizontal stress rotation (Zoback, Mazzotti and Townend). The large-magnitude earthquakes in the CSZ are concentrated outside the crater, but on the major rift faults, while the small-magnitude earthquakes are located within and beneath the crater region. Despite the high level of seismicity in the CSZ, only a few earthquakes are located on the southwestern part of the crater region (Fig. 1). In addition to the unique distribution of earthquakes in the CSZ, Mazzotti and Townend (2010) observed a significant clockwise rotation in the focal-mechanisms-derived horizontal stress orientation relative to the first-order regional stress orientation. Within the CSZ, stress inversion of focal mechanisms of the earthquakes on the northwestern cluster aligns with the first-order regional stress orientation while that of the southeastern cluster shows a significant clockwise rotation relative to the NW cluster (Mazzotti and Townend, 2010).

Numerical modeling is commonly used to explain earthquake distribution and the stress rotations. However, these numerical models require a realistic but simplified fault geometry due to the sensitivity of the modeled stress on the fault geometry. Previous work suggests two sets of geometries for the rift faults in the CSZ. One set has a uniform dip of 70°SE for all three faults (e.g. Baird et al., 2010), while the second set has 65°, 40°, and 40°SE, from north to south, respectively (Powell and Lamontagne, 2017). Fadugba et al. (2019) used the two fault geometries to model the stress state of the CSZ. Fadugba et al. (2019) observed differential correlations of modeled stress concentrations in the two fault geometries with observed seismicity and stress rotations, which might suggests along-strike variations in the dip angles of the rift faults. Visual estimation of fault planes from over 1300 relocated hypocenters in the CSZ (Powell and Lamontagne, 2017) suggests more complex fault geometry. An important research topic is whether pat-

89 pattern recognition algorithm can be used to determine simplified and realistic fault geom-
90 etry in the CSZ.

91 Several work has been done to determine realistic fault planes from the cloud of
92 hypocenters. For example, Ouillon et al. (2008) developed an Optimal Anisotropic Dy-
93 namic Clustering (OADC) analysis technique to delineate fault planes within the after-
94 shocks of the Parkfield earthquake sequences. The OADC method is a pattern recogni-
95 tion method aimed to reconstruct fault networks using the covariance of the spatial dis-
96 tribution of earthquakes from seismic catalogs. Ouillon and Sournette (2011) used the
97 Guassian kernel in a EM method to identify fault planes in intersecting cloud of seismic-
98 ity, hence intersecting fault planes. Wang et al. (2013b) extended the OADC method
99 to develop Anisotropic Clustering of Location Uncertainty Distributions (ACLUD). The
100 new ACLUD method incorporates some validation steps in order to give the best agree-
101 ment between the fault planes from a method similar to OADC to the observed focal mech-
102 anisms. They also used the uncertainty in the location of each earthquake in the cat-
103 alog instead of the threshold value assumed in Ouillon et al. (2008). The validation steps
104 proposed by Wang et al. (2013) produce several fault geometries that need the user's judg-
105 ment for discrimination.

106 Based on the assumption that modern seismicity in the CSZ illuminates active faults,
107 I will incorporate focal mechanisms to the Optimal Anisotropic Dynamic Clustering (OADC)
108 algorithm to determine realistic fault planes in the CSZ (Ouillon et al., 2008). I employ
109 a couple of hypotheses in this research. The first hypothesis is that modern seismicity
110 in the CSZ illuminates active faults and can be used to determine the number of the faults,
111 geometries and the interconnectivity of the fault system. The interconnectivity of these
112 faults can be used to predict the maximum magnitude earthquake in the CSZ (Harris
113 et al., 1991; Harris and Day, 1993). If modern earthquakes occur on active faults, then
114 the focal mechanisms of these earthquakes can be used to determine the style of fault-
115 ing e.g. strike-slip or reverse faulting. In other words, earthquake source mechanisms and
116 seismicity clusters define coherent fault surfaces, hence, the observed slip directions im-
117 plied by the mechanisms should also be coherent. Based on observed circular arcs of seis-
118 micity that follow the edge of the impact structure found in 3D tomographic inversions
119 (Fig. 1, Powell and Lamontagne, 2017), the second hypothesis is that the interface be-
120 tween the crater and the crust can slip and thus can cause earthquakes. High-resolution
121 focal mechanisms of moderate earthquakes (M2 – M4) will then be coupled with the Op-

122 optimal Anisotropic Dynamic Clustering (OADC) analysis technique to delineate realistic
 123 fault geometries. The derived fault geometry from this study will be incorporated in
 124 future geodynamic models to determine if the modeled stress result is consistent with
 125 the regional stress field and hence provide an explanation for the seismicity of CSZ.

126 **2 Methods**

127 We use the relocated hypocenters of Powell and Lamontagne (2017) in this study.
 128 Powell and Lamontagne (2017) relocated the hypocenters, to an error of less than 1 km,
 129 using the 3-D V_p and V_s velocity models determined from a travel time tomography study.
 130 Specifically, the hypocenters were relocated with horizontal and vertical errors of 0.15
 131 km and 0.35 km, respectively. Despite the high precision in hypocenter location, the hypocen-
 132 ter shows some unclustered hypocenter probably due to the damaged crustal rocks in
 133 the impact structure (Fig. ??).

134 The method used in this study can be broadly divided into two subsections. We
 135 first perform declustering analysis on the catalog to remove isolated and diffused earth-
 136 quakes, in order to highlight the rift faults in the CSZ. Based on the diffuse nature of
 137 the background seismicity recorded in the CSZ, the seismicity in the CSZ will be sep-
 138 arated into clustered and unclustered events based on the collapsing method (Jones and
 139 Stewart, 1997) and cumulative tetrahedra volume (Ouillon and Sornette, 2011). We then
 140 apply an Optimal Anisotropic Dynamic Clustering (OADC) algorithm to model realis-
 141 tic fault planes that best fit the hypocenter data.

142 In order to avoid spurious fault plane identifications, each cluster of events will be
 143 isolated before determining optimal fault planes that minimize the thickness of the clus-
 144 ter. This is necessary because the OADC method will tend to fit the hypocenters with
 145 a near-horizontal plane when the depth extent of the earthquakes in a cluster is far less
 146 than the areal extent of the cluster.

147 **2.1 Declustering analyses**

148 We used two techniques to decluster the hypocenters: a collapsing method (Jones
 149 and Stewart, 1997) and the cumulative distribution of tetrahedra volume method (Ouil-
 150 lon and Sornette, 2011). The collapsing method involves moving each hypocenter within
 151 its uncertainty ellipsoid making the collapsed hypocenters within acceptable error in the

152 earthquake location algorithm. The error ellipsoid is constructed with 99.86% confidence
 153 interval (i.e., 4 standard deviations). The idea of the cumulative distribution of tetra-
 154 hedra volume method is that the volume of a tetrahedral formed by four neighboring hypocen-
 155 ters of unclustered/isolated hypocenters will be higher than those of a clustered hypocen-
 156 ter. Given the small horizontal and vertical errors in the relocation catalog, and the dif-
 157 fuse nature of the seismicity, the cumulative distribution method has little success in sep-
 158 arating the clustered hypocenters. To solve this problem, we first applied the collaps-
 159 ing method on the catalog to reduce the variance of the earthquake distribution. and
 160 then apply the cumulative distribution method to remove any remaining isolated/unclustered
 161 hypocenters.

162 The collapsing method involves two loops: the first is on each hypocenter
 163 while the other loop is on each generation of collapsed hypocenters. We encourage the
 164 reader to see Jones and Stewart (1997) for more detailed description and limitations of
 165 the method. In summary, the collapsing method involves the following steps: (1) For each
 166 earthquake (object earthquake), we find all other earthquakes whose locations lie within
 167 the error ellipsoid of the object earthquake using $(\frac{x-x_0}{\sigma_x})^2 + (\frac{y-y_0}{\sigma_y})^2 + (\frac{z-z_0}{\sigma_z})^2 \leq s$,
 168 where s is related to the confidence interval at the specified degree of freedom. In this
 169 study, we use degree of freedom of 3, since the location of the hypocenters are in 3 di-
 170 mension. (2) Determine the centroid of the earthquakes including the object earthquake,
 171 and determine the distance and direction of the centroid to the object earthquake. We
 172 then move the object earthquake by a factor of 0.68103 of the distance and in the direc-
 173 tion to the calculated centroid (Press et al., 1986). The 0.68103 is necessary for stabil-
 174 ity (Jones and Stewart, 1997). The location of the object earthquake remains unchanged
 175 during this iteration, so the order the hypocenters are processed does not affect the re-
 176 sult.

177 The outer loop of the collapsing method involves statistical assessment of the move-
 178 ment of the hypocenters, using the following steps: (1) We store the new location of the
 179 hypocenters as a new generation of hypocenters. (2) We normalized the movement of
 180 object earthquake by corresponding standard deviation, and (3) compare the distribu-
 181 tion of the normalized movement with a theoretical chi distribution with degree of free-
 182 dom of 3. We used chi distribution instead of chi-square distribution because the move-
 183 ment of the hypocenters have been normalized by standard deviation. we then repeat
 184 the collapsing method for the next generation of collapsed hypocenters while the loca-

185 tions and sizes of the ellipsoids of uncertainty of the original hypocenter locations remain
 186 unchanged.

187 We then apply a cumulative distribution of tetrahedra volume method on the col-
 188 lapsed hypocenters to remove unclustered hypocenters. We compare the distribution of
 189 the volumes of the tetrahedra in the collapsed (natural) catalog to the distribution of
 190 tetrahedra formed from randomized hypocenters (catalog) in a domain similar to the nat-
 191 ural catalog. We generate the randomized catalog by randomizing the x, y and z coor-
 192 dinate of each hypocenter in the collapsed catalog. We randomized the hypocenter in
 193 depth as well because of the high number of hypocenters in the upper 15 km thus affect-
 194 ing the distribution of the tetrahedra volume in the randomized catalog. Ouillon and Sor-
 195 nette (2011) did not randomize the depth of the natural catalog. Following (Ouillon and
 196 Sornette, 2011), the cumulative distribution can be summarized as follows. (1) Deter-
 197 mine the volume (V) of tetrahedra formed with quadruplets of nearest neighbor events
 198 around each hypocenter using equation (??) for both the collapsed (V) and randomized
 199 (V_0) catalogs. An apparent challenge occurs when the four nearest neighbor of an iso-
 200 lated hypocenter are clustered. Hence, we used three surrounding hypocenters and the
 201 object earthquake to form the tetrahedra. (2) We determine the cumulative distributions
 202 of the volumes, i.e., $N(V)$ and $N_0(V_0)$. (3) We determine the volume (V_0) of the random-
 203 ized catalog corresponding to 5% quantile of the distribution, i.e., probability of 0.05.
 204 (4) We then remove all hypocenters in the natural catalog with $V > V_0$, under the as-
 205 sumption that the correlated hypocenters in the collapsed catalog have volumes smaller
 206 than the 5% quantile of the tetrahedra volume distribution in the randomized catalog.

$$V = \frac{1}{6} \times \begin{vmatrix} x_1 & y_1 & z_1 & 1 \\ x_2 & y_2 & z_2 & 1 \\ x_3 & y_3 & z_3 & 1 \\ x_4 & y_4 & z_4 & 1 \end{vmatrix} \quad (1)$$

207 2.2 Modified OADC algorithm

208 Ouillon et al., (2008) developed the OADC method to determine an optimal num-
 209 ber of clusters. OADC method is a generalization of the k-means method using randomly-
 210 seeded planes to partition hypocenters into clusters. In this algorithm, we set the min-
 211 imum (N_0) and maximum (N_{\max}) number of faults to use in the clustering analysis, in

addition to the maximum cluster thickness (Δ) allowed in the algorithm. The value of Δ should be the same order of magnitude as the maximum radius of uncertainty ellipsoid of the hypocenters.

The algorithm starts with N_0 fault with random positions, orientations, and sizes. The value of N_0 is one in this study. In this study, we set the N_0 , N_{\max} and Δ to one, five and 0.5 km, respectively. We chose a N_{\max} value of five to account for any along-strike variation of dip angles in the crater region (Fadugba et al., 2019). We partition each hypocenter into different clusters based on its distance to the fault(s). We then determine the covariance matrix (\mathbf{C} , equation ??) of each cluster. The idea of the algorithm is to iteratively determine optimal fault planes that minimize the maximum eigenvalues of the covariance matrix. We perform a principal component analysis on the covariance matrix of each cluster to determine its eigenvectors and eigenvalues. Under the assumption that earthquakes are uniformly distributed over a fault plane, we infer the fault length, width, and thickness from the eigenvalues and the corresponding eigenvectors (Ouillon et al., 2008). This analysis is repeated until the algorithm converges to a fixed geometry. The computation stops when the maximum value of λ_3 in all the clusters is less than the value of Δ .

$$\text{Covariance matrix, } \mathbf{C} = \begin{pmatrix} \sigma_x^2 & cov(x, y) & cov(x, z) \\ cov(x, y) & \sigma_y^2 & cov(y, z) \\ cov(x, z) & cov(y, z) & \sigma_z^2 \end{pmatrix} \quad (2)$$

According to Ouillon et al., 2008, we attribute the largest eigenvalues (λ_1) to the length of the cluster, and the azimuth of the corresponding eigenvector to represent the strike of the fault. In addition, we use the intermediate (λ_2) and smallest (λ_3) eigenvalues to infer the width and thickness of the fault planes, respectively. The barycenter of each cluster (e.g., $x_b = \text{mean}(x)$) coincides with the center of the fault. Based on a statistical method, Ouillon et al., (2008) estimated the length (L) and width (W) of the fault plane using $\lambda_1\sqrt{12}$ and $\lambda_2\sqrt{12}$, respectively. The value of λ_3 gives information on the thickness of the cluster. The strikes and dips of the fault planes are determined from the eigenvector of the minimum eigenvalue (λ_3) of each cluster.

However, if the maximum λ_3 in the stable fault geometry is greater than Δ , the fault in thickest cluster is replaced by at least two new faults with random locations and

240 orientations within the cluster. The lengths of the new faults are one-half that of the orig-
 241 inal thick fault. We perform the splitting process several times (20 times in this study)
 242 to determine the random fault geometry that gives the least maximum λ_3 at the result-
 243 ing fixed geometry. The number of fault increases by one, and the covariance matrix anal-
 244 ysis is repeated. The simulation stops when the value of λ_3 is less than the value of Δ ,
 245 or the N_{\max} is reached.

246 In this study, we incorporate the focal mechanisms into the OADC algorithm to
 247 split the 'thick' cluster instead of using a randomly-seeded planes. We use any available
 248 high-quality focal mechanisms of earthquakes that are within or at a distance of 1 km
 249 to the thick cluster. We assign the first two dominant strike direction of the focal mech-
 250 anisms and the average of their corresponding dips to two faults. Wang et al., 2013 also
 251 incorporate focal mechanisms to OADC in their the ACLUD method, but as a valida-
 252 tion step after determining several results from OADC-type algorithm.

253 The idea is to plot the nodal plane normal vectors for earthquakes with high-quality
 254 source mechanisms and use the dominant orientations to specify the planes in the OADC
 255 method rather than using randomly-seeded planes.

256 3 Results

257 3.1 Declustering analyses

258 3.1.1 Modified collapsing method

259 The relocated hypocenters shows a thicker cloud of seismicity about the rift faults
 260 and some earthquakes appear to rim around the impact structure (Fig. 2C).

258 **Figure 2.** (A) Relocated earthquake distribution of the CSZ (Powell and Lamontagne, 2017),
 259 and (B) a theoretical scaled chi distribution.

261 In order to reduce the thickness of the clusters, we applied the collapsing method
 262 to account for the location errors in the hypocenters (Jones and Stewart, 1997). Figure
 263 – and – show the result of the collapsing method at 10th and 20th iteration, respec-
 264 tively, and the normalized movement of each hypocenter relative to its original location.

Figure 3. (A) Collapsed earthquake distribution at iteration number 10, and (B) the movement of the hypocenters compared with the theoretical scaled chi distribution.

Figure 4. Same as figure – but at an iteration number of 20.

The collapsing method has clustered some of the hypocenters. We stopped the iteration at 20 even though the hypocenter movements has not fitted the theoretical chi distribution. This is because the objective of collapsing method in this study is to reduce the variability in the hypocenter location, and not to totally collapse the hypocenters. The collapsing method at higher iterations and higher scaling factors of the uncertainty ellipsoid collapsed the earthquakes on a a rift fault to a line thereby affecting its depth information significantly. This may be due to the higher standard error in he z-direction.

We then applied the cumulative distribution method on the collapsed catalog to remove some of the hypocenters that are isolated.

3.1.2 Cumulative distribution of tetrahedra volume

We determine the volume of the tetrahedra for each earthquake in the 3D joint relocation of the 1329 earthquakes in the CSZ (Fig. 2A, Powell and Lamontagne, 2017). We first generated the randomized catalog within the domain size similar to the seismic zone (Fig.). The volumes of the tetrahedra ranges from 10^{-20} to about 31.61 km^3 . The very small lower bound of the volumes is because of the earthquakes that are co-located due to the collapsing method. We clipped the lower bound of the tetrahedra volumes at 10^{-5} km^3 (Fig.). The tetrahedra volume in the randomized catalog ranges from 0.0015 to 31.05 km^3 . The similarity in the maximum tetrahedra volume further supports the need to apply collapse method before the cumulative distribution of tetrahedra volume.

We determine the cumulative distribution function (CDF) of the tetrahedra volume of both catalogs (Fig. 3). The volume at 5 percent probability (V_{05}) is 0.099 km^3 and the probability at target volume ($N(V_{05})$) = 0.7223. This method removes 370 unclustered earthquakes (27.84% of the original catalog). Figure 2B shows the collapsed and clustered hypocenters while figure 2C shows highlights the unclustered hypocenters.

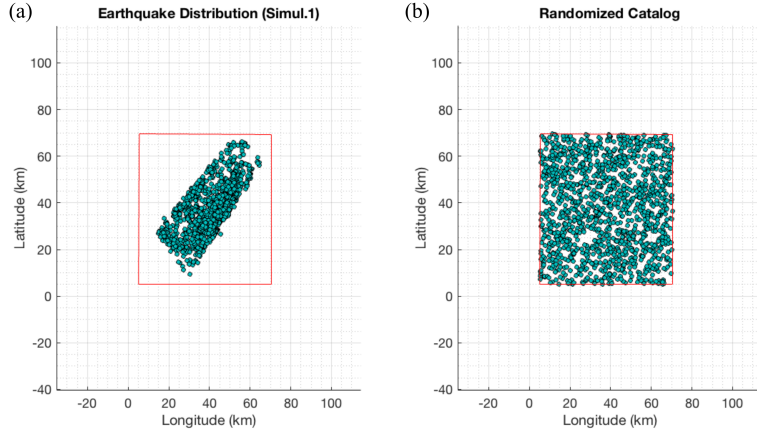


Figure 5. Domain of randomized catalog.

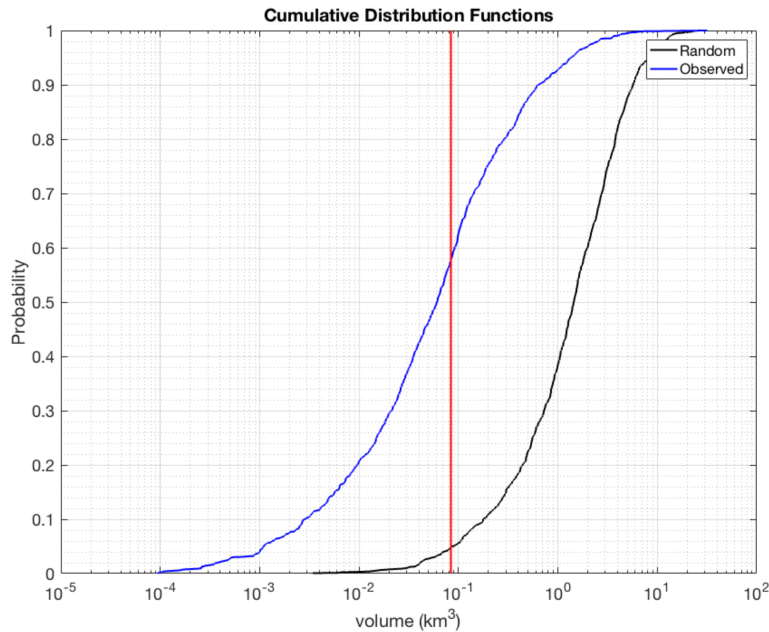


Figure 6. cumulative distribution curve for hypocenters of the earthquakes of the CSZ.

The clustered and unclustered hypocenters give interesting incite to the seismicity of the CSZ. For example, the clustered hypocenters occur on identifiable alignment related to the main rift faults in the CSZ, and have been enhanced compared to the full relocated hypocenters of Powell and Lamontagne (2017) (compare figures 2A and 7B). The clustered earthquakes also reveal a curvature of hypocenters in the western part of the seismicity distribution probably following the boundary of the crater. The unclustered earthquakes are random showing no significant alignment which may depict con-

297 centration of hypocenters on rift faults (Fig. 2D). However, the unclustered earthquakes
 298 are more in the impact structure than on those near the rift faults.

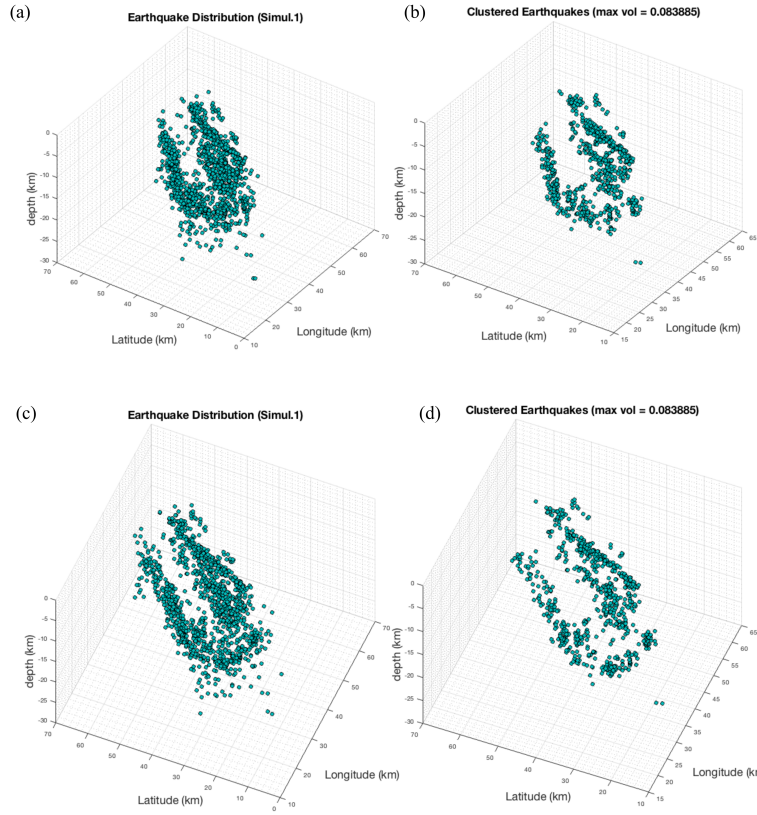
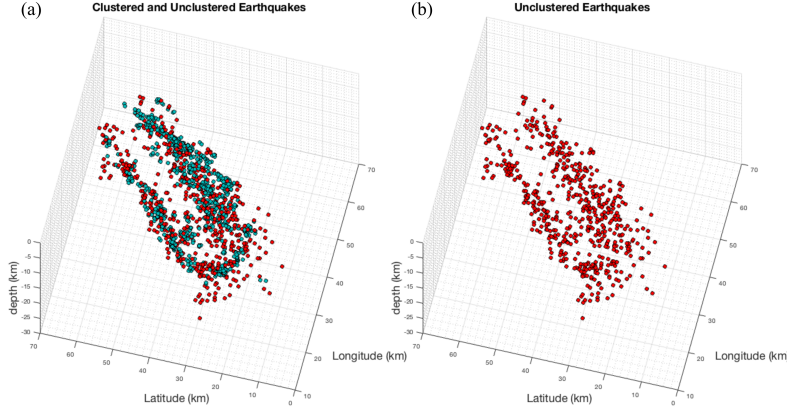


Figure 7. Clustering of earthquakes in CSZ using modified cumulative distribution method.

3.2 Fault plane geometry of the CSZ

300 The best-fit fault planes from the modified OADC algorithm are geologically fea-
 301 sible (Fig. 6). Figures 6A and 6B show the intermediate fault models using 1 and 3 fault
 302 planes, respectively. The one-fault intermediate model fit the clustered hypocenter but
 303 with a large minimum eigenvalue compared to the input threshold (0.001 km) (Fig. 6A).
 304 The fault was splitted, the OADC algorithm is repeated. When the number i faults is
 305 3, the OADC algorithm was fitted one fault to the NW and SE clusters, and also fitted
 306 the earthquakes beneath the crater with a near-horizontal fault (Fig. 6B).

307 The best fit occur when the number of faults is 5 (Fig. 6C and D). The OADC fit-
 308 ted the SE cluster with two fault planes with dips 43.9° and 42.8° , respectively. The NW

**Figure 8.** Unclustered hypocenters.**Table 1.** Fault geometry of the CSZ using OADC method.

Fault No	Strike	Dip	Possible mapped fault
1	65.8°	43.9°	Saint-Laurent fault
2	56.4°	42.8°	Charlevoix fault
3	82.1°	33.5°	Crater boundary
4	30.3°	34.8°	Crater boundary
5	50.0°	60.0°	Gouffre Northwest fault

309 cluster was fitted with a steeper faults with a dip of 60°. Within the crater region, OADC
 310 fitted two more faults with shallower dips: 33.5° and 34.8°. The shallower dip planes are
 311 probably in response to the earthquakes wrapping around the crater region. Table 1
 312 shows the summary of fault geometry from the OADC algorithm.

313 4 Discussion

314 In this section, we will discuss the unclustered and clustered hypocenters, and the
 315 limitations of the OADC from this study.

316 4.1 Unclustered seismicity

317 *The removal of the Unclustered seismicity decrease the fuzziness of earth-
 318 quake distribution in the CSZ, thereby highlighting the rift faults (Figs. 2A*

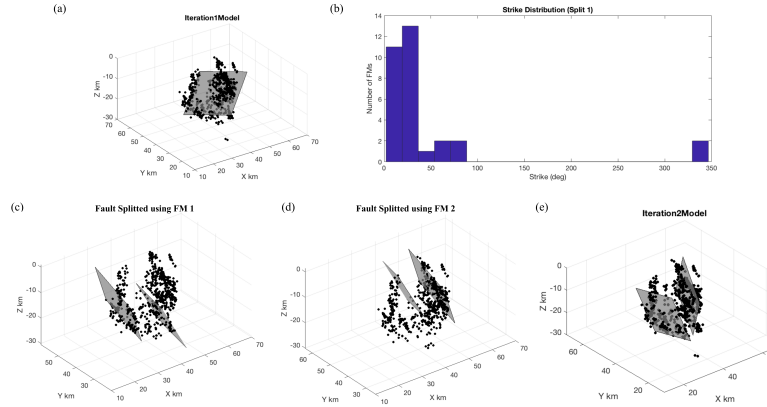


Figure 9. Intermediate fault models of OADC method on the clustered earthquakes.

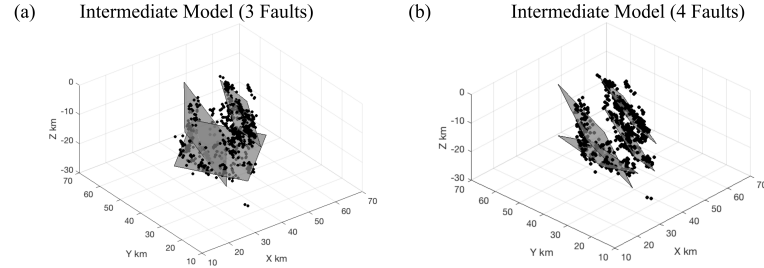


Figure 10. Intermediate fault models of OADC method on the clustered earthquakes.

319 **and C).** The unclustered earthquakes do not have inherent structure showing the rift
 320 faults, which suggests that they do not occurred on the major rift faults in the CSZ. The
 321 lack of inherent alignment validate the declustering method has not removing clustered
 322 hypocenters. Powell and Lamontagne (2017) also shows that the rift faults can not be
 323 traced inside the crater region. In this method removes the fuzziness of the seismicity
 324 within the crater and thus, the faults can be followed all the crater within the crater re-
 325 gion. Thereby, helps to constrain the geometry of the rift faults (Fig. 2C).

326 **The unclustered seismicity in the crater region shows the geometry of**
 327 **the crater (Figs. 2B and D).** The unclustered seismicity in the crater region is the
 328 background seismicity, and is mainly within the crater region. These background seis-
 329 micity highlights the damaged region of the crater (the inner circle in Figure 1). *Cre-*
 330 *ate a 3D map of the removed seismicity to highlight the geometry of the crater.*

331 **Figure of the background seismicity showing the inner circle.**

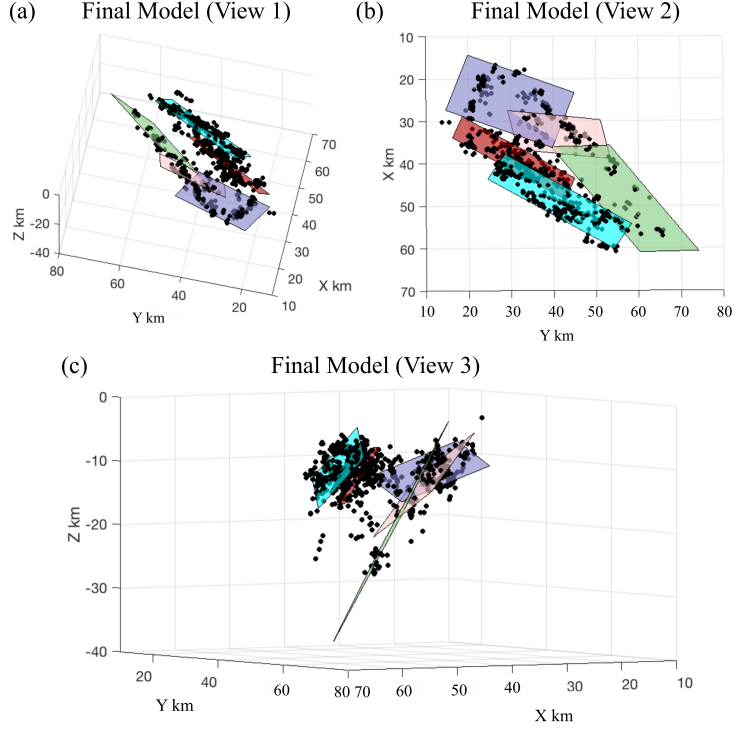


Figure 11. Final fault models of OADC method on the clustered earthquakes.

332 4.2 Clustered seismicity

333 *The clustered seismicity show identifiable planes revealing the geometry of the three major rift faults in the CSZ (Fig. 3D).* The first fault dips at
 334 an angle of 60° while the other two main rift faults dip at 44° and 43° , respectively (Fig.
 335 4D). We need to plot the clustered earthquakes on a geologic map to see the difference.
 336 And also plot some cross-sections. The results from this study also support Powell and
 337 Lamontagne (2017) that the alignment of the earthquakes on identifiable planes suggests
 338 that the earthquakes occurred on the rift faults instead of concentrating within the fault
 339 volume as suggested by previous authors (e.g. Baird et al. 2010, Auglin, Lamontagne,
 340 Rondot). These fault geometries match the work by Powell and Lamontagne (2017). The
 341 rift faults in the OADC supports that the South Shore fault do not play a role in the seis-
 342 micity of the CSZ.
 343

344 *In addition to the simple geometry of the rift faults, the seismicity re-*
 345 *veals a more complicated geometry (Fig. 4D). There is a change in the strike*
 346 *of the rift faults.* Similar to what we see on the fault trace on Figure 1. Within the

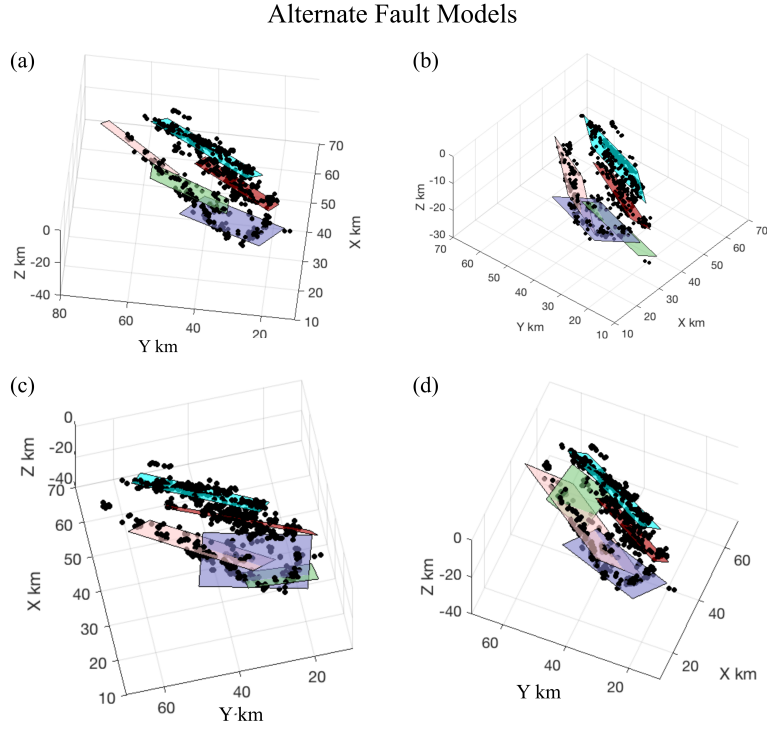


Figure 12. Alternate fault models of OADC method.

347 crater region, the faults are farther apart and somewhat converge in the northeastern
 348 part of the seismic zone. The middle and Charlevoix fault are closer outside the crater
 349 region. This is contrary to the simple fault geometry employed in Fadugba et al. (2010)
 350 with constant distance separation between the rift faults.

351 *And also reveals a change of dip in the first rift faults (Fig. 3D).* in the
 352 form of three segments. Outside the crater, the first rift fault follow the first order strikes
 353 of the rift faults. Along strike variation in the dip of the rift faults (Fadugba et al., 2019).
 354 Within the crater region, the faults dips at 33.4° and 34.8° .

355 *The seismicity follows the crater boundary (Fig. 3D).* especially well in the
 356 northeastern part of the crater, and the shows that the seismicity also wrap around and
 357 beneath the crater. This seismicity highlights the geometry of the crater thereby con-
 358 straining the depth of the crater.

359 Lambda3 is better to solve fitting horizontal plane fit. Show two figures showing
 360 fit with both lambda3 and global variance.

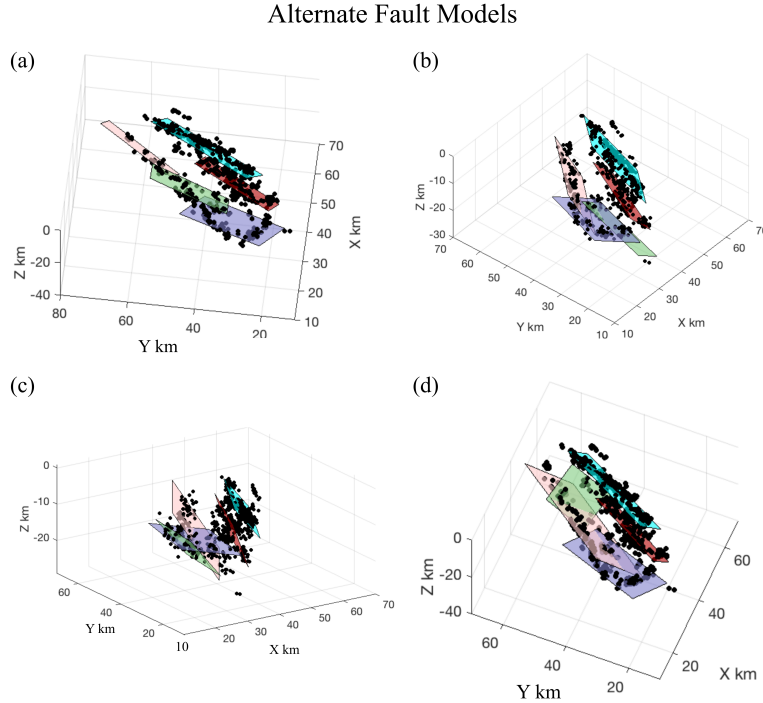


Figure 13. Alternate fault models of OADC method.

4.3 Limitation of OADC

The results of OADC algorithm may change for every run because the results depend on the initially random seed planes within each cluster. Therefore, we may need to repeat the algorithm several time until the fault geometry is geologically feasible.

The surface projection of the fault planes from OADC may not coincide the fault trace on the geologic map. We need to find out how it changes.

5 Conclusions

The first fault dips at an angle of 60° while the other two main rift faults dip at 44° and 43° , respectively. These fault geometries match the work by Powell and Lamontagne (2017). The rift faults show a more complicated geometry than the simple three-faults model in previous works, especially within the crater region. Within the crater region, the faults dips at 33.4° and 34.8° .

374 **Acronyms**

375 **CSZ** Charlevoix Seismic Zone

376 **SH_{max}** Maximum horizontal principal stress

377 **OADC** Optimal Anisotropic Dynamic Clustering

378 **ACLUD** Anisotropic Clustering of Location Uncertainty Distributions

379 **CDF** Cumulative Distribution Function

380 **Acknowledgments**

381 This research was supported by Center for Earthquake Research and Information, Uni-
382 versity of Memphis.